Flexible Thermal Conductance Model (TCM) for Efficient Thermal Simulation of 3-D ICs and Packages

Shunxiang Lan[1], Min Tang[1], and Jun Ma[2]
[1]State Key Laboratory of Radio Frequency Heterogeneous Integration, SJTU, Shanghai, China
[2]School of Mathematical Science, SJTU, Shanghai, China
tm222@sjtu.edu.cn

***Abstract*—Thermal management plays an increasingly important role in the design of 3-D integrated circuits (ICs) and packages. To deal with the related thermal issues, efficient and accurate evaluation of the thermal performance is obviously essential. In this paper, an efficient approach with the flexible thermal conductance model (TCM) is presented for thermal simulation of 3-D ICs and packages. Firstly, the entire structure is partitioned and classified into two kinds of regions, named region of interest (ROI) and region of fixity (ROF). The ROI usually contains the key components in thermal designs while the ROF holds invariant thermal characteristics. Then, in order to represent the thermal impact of ROF on ROI, a novel technique based on the TCM is developed, which can be treated as the equivalent boundary condition of the ROI. By this means, the solution domain of the whole system is constrained to the ROI, which results in significant reduction of computational costs. Furthermore, in the representation of ROF, a flexible TCM with elegant rational expressions on the heat convection coefficient is proposed to deal with varying boundary conditions, which greatly expands the applicability of this method. The validity and efficiency of the proposed method is illustrated by the numerical examples, where a 138x speedup is achieved comparing with the commercial software.**

***Index Terms*—Convection boundary condition, thermal conductance model (TCM), integrated circuit (IC), package, thermal simulation.**

I. Introduction

With the continued reduction in critical dimension of very large scale integrated circuits, the system performance of integrated circuits (ICs) depends heavily on the performance of interconnections [1]. 3-D ICs innovatively employ through-silicon vias (TSVs) and micro-bumps for vertical interconnections, significantly shortening wire lengths and therefore reducing interconnection latency [2]. While 3-D technology undoubtedly provides notable advantages in terms of electrical performance, it also compounds the already formidable issue of microelectronics cooling [3]. The increased heat generation in a concentrated area inevitably results in a higher hotspot temperature, which may lead to performance degradation and even physical damage [4]. Thus, it is essential to perform comprehensive thermal analysis and management of 3-D ICs and packages in the early stage of the design to ensure the system reliability.

In the past few decades, various numerical methods have been proposed for solving the heat conduction problems, such as the finite element method (FEM) and finite volume method (FVM). In recent years, the boundary condition independent (BCI) compact thermal models (CTMs) have been proven to be a powerful tool to evaluate the thermal performance of 3-D ICs and packages. Based on the multi-point moment matching technique, a model order reduction approach is presented in [5] for transient simulation with a desired level of accuracy. Moreover, a fast novel thermal analysis simulation tool for integrated circuits (FANTASTIC) [6] with fixed boundary conditions is extended to the BCI CTMs using the Galerkin's projection framework [7]. Compared to the previous work, this method can automatically generate both static and dynamic BCI CTMs with required accuracy and a parametric set of Robin boundary conditions. However, the efficiency of the above methods will deteriorate when extracting the BCI CTMs of structures with multiple heat sources.

In [8], another efficient method based on domain decomposition and the thermal resistance network derivative (TREND) model is proposed. This approach divides the entire system into core regions and non-core regions according to the specific structural characteristic. The TREND model contributes to focusing the solution domain on the core regions for thermal design and accelerating simulation without sacrificing accuracy. However, this method has two main drawbacks. Firstly, it may encounter failure during the TREND model extraction if all the surfaces and interfaces belong to the second kind boundary. Secondly, once the boundary conditions of the non-core area change, the TREND model must be re-extracted to ensure the accuracy, which is detrimental to efficient thermal design.

To overcome the above limitations, we present a flexible thermal conductance model (TCM) to achieve efficient thermal simulation of 3-D ICs and packages. The main contributions of our work are summarized as follows:

- We illustrate a strategic approach for region decomposition. It divides the entire system into several subsystems according to the specific requirements of thermal design, which is beneficial for establishing the TCM and parallel computation.
- We propose a novel TCM to characterize the thermal interplay at the interface of linear time-invariant systems in the form of equivalent boundary conditions. By this means, the solution domain is reduced from the entire system to the core region, therefore significantly improving the efficiency.

978-3-9826741-0-0/DATE25/© 2025 EDAA

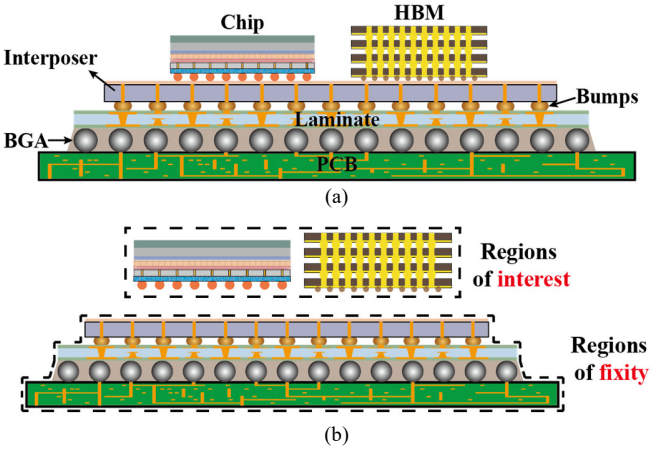

Fig. 1. Region decomposition of a typical system of 3-D ICs and packages.

- We present an innovative approach to efficiently estimate the thermal behaviors under different convection scenarios. Based on the mathematical derivation, a flexible TCM associated with the heat convection coefficient is achieved with elegant rational expressions, which is convenient to deal with varying boundary conditions and thus greatly expands the applicability of this method.
- We demonstrate the advantages of the proposed method by two numerical examples. The first example illustrates how to utilize the flexible TCM to conduct modular thermal design. Then, a high-performance server system-on-chip (SoC) case is provided to validate the accuracy and efficiency of the proposed method. Compared with the commercial software, a speedup of 138x is achieved with satisfactory accuracy.

II. Development of the Proposed Method

A. Region Decomposition

For a typical system of 3-D ICs and packages shown in Fig. 1(a), the temperature rise within the silicon-based chip and high bandwidth memory (HBM) is of vital guiding significance due to its strong impacts on the performance, reliability, and lifespan of the system. In contrast, the packaging and interconnection structures do not contain the active components and have relatively weak relation to the hotspot of the system.

According to the degree of importance discussed above, the entire system can be decomposed into two parts: regions of interest (ROIs) and regions of fixity (ROFs), as illustrated in Fig. 1(b). The ROIs usually encompass the temperature profiles of critical high-power ICs, which are the most important parts in the thermal design. On the other hand, the ROFs typically contain large-scale package structures, which can be treated as a linear time-invariable system where the model parameters within the ROFs remain fixed during the thermal design process.

B. Thermal Conductance Model

To reduce the solution domain and focus on the ROIs, we introduce a novel TCM to represent the impact of ROFs on ROIs in the form of equivalent boundary conditions, as illustrated in Fig. 2.

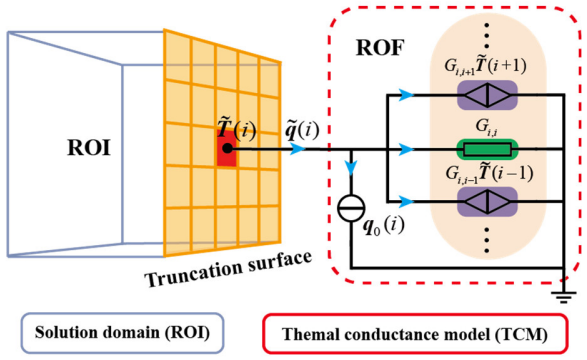

Fig. 2. Schematic of the thermal conductance model.

Firstly, the truncation surface between the ROF and the ROI is imposed with an isothermal boundary condition. For simplicity without loss of generality, we set $T = 0$ K on the truncation surface, such that the temperature rise on the truncation surface is equal to the temperature value. Then, the FVM is applied to obtain the corresponding heat flux density $\boldsymbol{q}_0$ on the truncation surface.

Next, assuming that there are M face elements on the truncation surface, we apply a temperature excitation to each face element one by one. When T_j is imposed on the j-th (j = 1, 2, …, M) face element, the responding heat flux density $\boldsymbol{q}_j$ of all the face elements on the truncation surface can be calculated. In theory, a well-posed problem is certainly constructed due to the isothermal boundary on the truncation surface. By contrast, the TREND model [8] may encounter failure since the truncation surface belongs to the second kind boundary in the derivation process. It is the main advantage of TCM over the TREND model.

After $\boldsymbol{q}_j$ is obtained, the equivalent thermal conductance G_{ij} from the j-th face element to the i-th (i = 1, 2, …, M) one is defined as

$$G_{ij} = \frac{S_i}{S_j} \cdot \frac{\boldsymbol{q}_j(i) - \boldsymbol{q}_0(i)}{T_j} \tag{1}$$

where S_i and S_j represent the areas of the i-th and j-th face elements, respectively.

Then, according to the superposition principle of linear time-invariant systems, the mapping relationship between the temperature distribution $\tilde{\boldsymbol{T}}$ and the resulting heat flux density $\tilde{\boldsymbol{q}}$ on the truncation surface is constructed as

$$\tilde{\boldsymbol{q}} - \boldsymbol{q}_0 = \boldsymbol{G}\tilde{\boldsymbol{T}} \tag{2}$$

where $\boldsymbol{G}$ is an $M \times M$ equivalent thermal conductance matrix calculated by (1). The relationship described in (2) is represented by the equivalent circuit named TCM. For example, the local TCM of the i-th face element on the truncation surface is demonstrated in Fig. 2. The heat flux difference $\tilde{\boldsymbol{q}}(i) - \boldsymbol{q}_0(i)$ is induced by two kinds of contributions: the self-heating effect and the mutual heating effect. According to the similarity between the thermal field and electric field, the two effects are represented by the current through G_{ii} and a series of voltage-controlled current sources, respectively.

Subsequently, to replace the impact of the ROF in the original system, we impose (2) on the truncation surface of the ROI

as the Robin boundary condition. The ROI is then solely simulated using the traditional FVM.

In summary, following the above process, this approach successfully reduces the solution domain from the entire system to the ROI and focuses on solving the most interesting temperature results for thermal design, which is rather beneficial for improving the efficiency.

C. Flexible TCM

In practice, investigating the thermal performance under different air-cooling conditions is a common requirement for thermal design. Therefore, to expand the capability of TCM and facilitate its reusability under varying convection boundary conditions, we develop a novel flexible TCM.

Firstly, the impact of the convection coefficient h on the temperature field is investigated. A typical convection boundary condition is given by

$$q = h(T - T^{amb}) \tag{3}$$

where h is the convection coefficient and T^{amb} is the ambient temperature.

Then, when h approaches positive infinity, that is, the convection boundary condition in (3) is transformed into an isothermal boundary condition as $T = T^{amb}$, we apply the FVM to obtain the corresponding matrix equation

$$\boldsymbol{A}\boldsymbol{x} = \boldsymbol{b} \tag{4}$$

where $\boldsymbol{A}$ is an $N \times N$ stiffness matrix (N is the total number of volume elements), $\boldsymbol{b}$ is an $N \times 1$ right-hand side vector, and $\boldsymbol{x}$ represents the temperature values when h tends to infinity.

Next, as for a normal value of h, assuming that there are N_C face elements on the convection boundary, the matrix equation in (4) is modified as

$$\left(\boldsymbol{A} - \boldsymbol{H}\right)\bar{\boldsymbol{x}} = \boldsymbol{b} - \boldsymbol{H}\boldsymbol{T}^{amb} \tag{5}$$

where

$$\boldsymbol{H} = \begin{bmatrix} \boldsymbol{H}_C & \boldsymbol{0} \\ \boldsymbol{0} & \boldsymbol{0} \end{bmatrix} \tag{6}$$

$$\boldsymbol{T}^{amb} = \begin{bmatrix} \boldsymbol{T}_C^{amb} & \boldsymbol{0} \end{bmatrix}^T \tag{7}$$

Here, $\boldsymbol{T}_C^{amb}$ is a $1 \times N_C$ vector with all the elements equal to T^{amb} and $\boldsymbol{H}_C$ is an $N_C \times N_C$ diagonal matrix with the element

$$h_k = \frac{S_k \times \left(\kappa_k / L_k\right)^2}{h + \left(\kappa_k / L_k\right)} \quad \left(k = 1, 2, \cdots, N_C\right) \tag{8}$$

where S_k is the area of the k-th face element on the convection boundary, L_k is the distance between the center of the k-th face element and the center of the adjacent volume element, and κ_k is the thermal conductivity of the k-th face element.

Subsequently, combining (4) and (5), we obtain

$$\bar{\boldsymbol{x}} = \boldsymbol{x} + \boldsymbol{A}^{-1}\boldsymbol{H}(\bar{\boldsymbol{x}} - \boldsymbol{T}^{amb}) . \tag{9}$$

Therefore, the p-th (p = 1, 2, …, N) element in $\bar{\boldsymbol{x}}$ can be expressed as

$$\bar{x}_p = x_p + \sum_{k=1}^{N_C} \frac{a_{pk} m_k}{h + l_k} \tag{10}$$

where

$$m_k = S_k \times l_k^{\,2} \times \left(\bar{x}_k - T^{amb}\right) \tag{11}$$

$$l_k = \kappa_k / L_k \tag{12}$$

and a_{pk} is the element of matrix $\boldsymbol{A}^{-1}$.

Further, according to the relationship of (1), the heat flux density can be considered as a linear function of temperature variable from the mathematical point of view. Therefore, combining (1) and (10), the impact of the convection coefficient can be approximately transferred onto the equivalent thermal conductance matrix, as given by the following rational expression:

$$G_{ij}(h) = G'_{ij} - \sum_{k=1}^{N_C} \frac{m'_{ij,k}}{h + l'_{ij,k}} \tag{13}$$

where G'_{ij}, $m'_{ij,k}$, and $l'_{ij,k}$ are the coefficients. Note that the determination of these coefficients is not an easy task. Fortunately, in practice, we only need to calculate a few terms in (13) to achieve satisfactory accuracy under varying convection boundary conditions.

For simplicity without the loss of generality, we only consider one term in the rational expression of (13), which is written as

$$G_{ij}(h) = G'_{ij} - \frac{m'_{ij}}{h + l'_{ij}} \qquad h \in (h^{min}, h^{max}) \tag{14}$$

where h^{min} and h^{max} are the lower and upper limits of the convection coefficients in the thermal design, respectively.

To determine the values of the coefficients G'_{ij}, m'_{ij}, and l'_{ij}, we construct three TCMs of ROFs as described in Section II-B corresponding to the scenarios with fixed convection coefficients (e.g., h^{min}, h^{max}, and h^{inter}). Here, the empirical value of h^{inter} is given by

$$h^{inter} = \sqrt{h^{min} h^{max}} . \tag{15}$$

The resulting equivalent thermal conductance matrices are $\boldsymbol{G}^{min}$, $\boldsymbol{G}^{max}$, and $\boldsymbol{G}^{inter}$, respectively.

Then, combining with (14), we calculate the value of the coefficients as

$$\begin{aligned} G'_{ij} = \frac{1}{d_{ij}} \Big[& \left(h^{min} - h^{max}\right) G_{ij}^{min} G_{ij}^{max} + \left(h^{max} - h^{inter}\right) G_{ij}^{max} G_{ij}^{inter} \\ & + \left(h^{inter} - h^{min}\right) G_{ij}^{inter} G_{ij}^{min} \Big] \end{aligned} \tag{16}$$

$$\begin{aligned} m'_{ij} = \frac{f}{d_{ij}^2} \Big[& \left(G_{ij}^{max}\right)^2 \left(G_{ij}^{min} - G_{ij}^{inter}\right) + \left(G_{ij}^{inter}\right)^2 \left(G_{ij}^{max} - G_{ij}^{min}\right) \\ & + \left(G_{ij}^{min}\right)^2 \left(G_{ij}^{inter} - G_{ij}^{max}\right) \Big] \end{aligned} \tag{17}$$

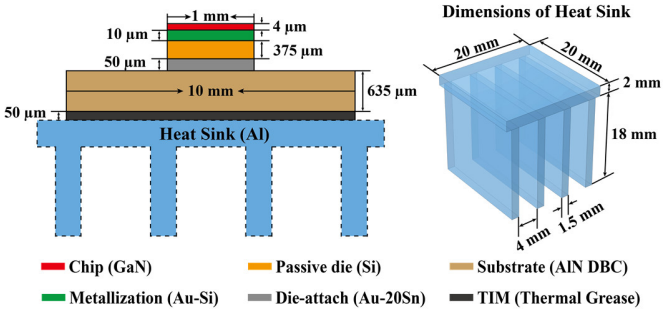

Fig. 3. Schematic of the typical structure of stacked ICs with heat sink.

$$l'_{ij}=\frac{1}{d_{ij}}\Big[(h^{inter}-h^{min})h^{max}G_{ij}^{max}+\left(h^{min}-h^{max}\right)h^{inter}G_{ij}^{inter} +\left(h^{max}-h^{inter}\right)h^{min}G_{ij}^{min}\Big] \tag{18}$$

where

$$d_{ij}=\left(h^{min}-h^{inter}\right)G_{ij}^{max}+\left(h^{max}-h^{min}\right)G_{ij}^{inter} +\left(h^{inter}-h^{max}\right)G_{ij}^{min} \tag{19}$$

and

$$f=\left(h^{max}\right)^2\left(h^{min}-h^{inter}\right)+\left(h^{inter}\right)^2\left(h^{max}-h^{min}\right) +\left(h^{min}\right)^2\left(h^{inter}-h^{max}\right). \tag{20}$$

By this means, we finally achieve a flexible TCM described in (14). This approach efficiently constructs the TCM under varying convection boundary conditions, which facilitates flexible thermal design of 3-D ICs and packages. In practice, a flexible TCM with only one term (as shown in (14)) can achieve satisfactory accuracy. Note that the accuracy can be further enhanced when more terms are utilized in the rational expression. Correspondingly, we need to construct more TCMs with different convection coefficients in the interesting range of thermal design.

III. Numerical Results

In this section, two numerical examples are provided to evaluate the performance of the proposed method. All simulations are performed on a server with two Intel Xeon Platinum 8268 CPUs (2.90 GHz/2.89 GHz) and 1.0-TB memory.

A. 3-D Stacked ICs with Heat Sink

To demonstrate the advantages of the proposed method, a typical example of 3-D stacked ICs with heat sink is investigated. The structure is depicted in Fig. 3 and the material properties are referred to [9]. The surface of the heat sink is imposed with the convection boundary and an ambient temperature is 300 K. All other surfaces are assumed to be adiabatic.

For the purpose of thermal design, we need to evaluate the impacts of both material properties and die-attach thickness on the hotspot temperature with different chip powers under the scenario of varying convection boundary conditions. To fulfill this requirement, we will conduct thermal simulations for 686 cases in total.

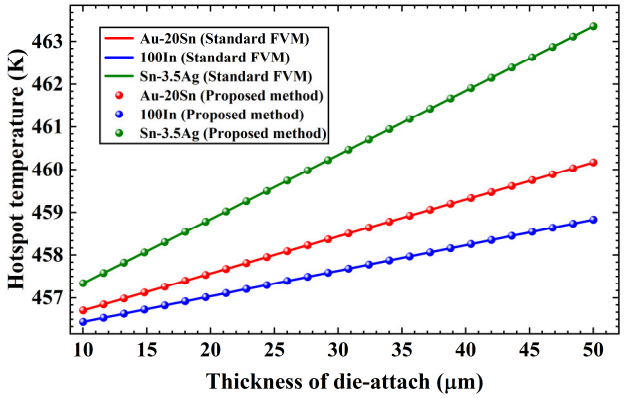

Fig. 4. Impact of die-attach thickness and material on the hotspot temperature when the chip power is 5 W.

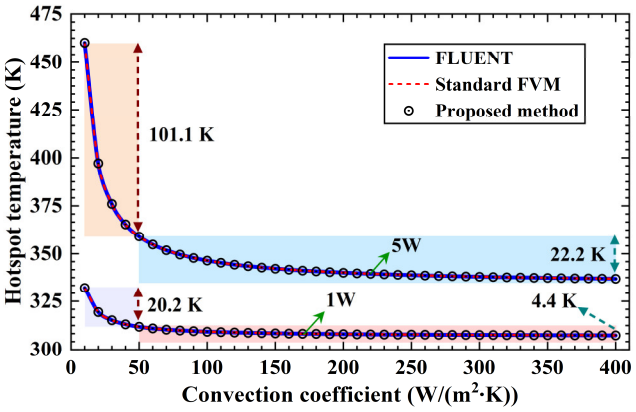

Fig. 5. Impact of the convection coefficient on the hotspot temperature with 1 W and 5 W chip powers.

TABLE I
Comparison of CPU Time

	Pre-simulation	Simulation
FLUENT	None	25 h 49 m 13 s
Standard FVM	None	18 h 42 m 8 s
Proposed method	3 m 9 s	8 m 5 s

Firstly, we decompose the entire system into two parts. Part one is the ROI, containing the chip, metallization, die and die-attach. Part two is the ROF, encompassing the substrate, TIM and heat sink.

Then, we consider the thermal design with the chip power of 5 W under the environment of the natural convection condition with h = 10 W/(m^2·K). Based on the TCM, we only need to concentrate on the ROI, thus the influence of the die-attach thickness with different materials on the hotspot can be investigated efficiently. The results are described in Fig. 4. It is seen that the hotspot temperature increases almost linearly with the thickness of die-attach for different material cases. To illustrate the accuracy of the proposed TCM, the standard FVM (where both the ROI and ROF are simulated) is performed for reference. We observe that they are in excellent agreement with each other. The maximum error is less than 10^{-4} K, which implies that there is almost no accuracy loss by utilizing the TCM to conduct thermal simulations. Then, we

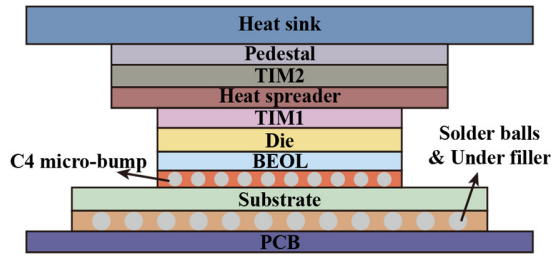

Fig. 6. Schematic of the cross-section of the high-performance server SoC.

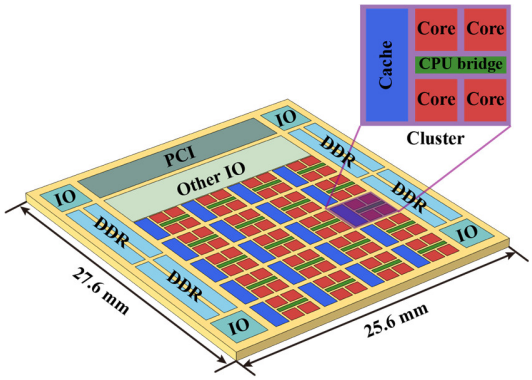

Fig. 7. 3-D display of the commercial SoC with 1 peripheral component interconnect (PCI), 4 inputs/outputs (IOs), 8 double data rate (DDR) controllers and 20 clusters [12].

consider the thermal design with the chip power of 5 W under the natural convection condition with h = 10 W/(m^2·K). Based on the TCM, we only need to concentrate on the ROI, thus the influence of the die-attach thickness with different materials on the hotspot can be investigated efficiently. The results are described in Fig. 4. It is seen that the hotspot temperature increases almost linearly with the thickness of die-attach for different material cases. To illustrate the accuracy of the proposed TCM, the standard FVM (where both the ROI and ROF are simulated) is performed for reference. We observe that they are in excellent agreement with each other. The maximum error is less than 10^{-4} K, which implies that there is almost no accuracy loss by utilizing the TCM to conduct thermal simulations.

Then, the flexible TCM is employed to investigate the thermal performance when the convection coefficient h varies from 10 W/(m^2·K) to 400 W/(m^2·K). Here, only one term is employed in the rational expression of the flexible TCM, as described in (14). The results obtained by the proposed method are compared to those of ANSYS FLUENT [10] and the standard FVM in Fig. 5. It is observed that when h increases from 10 W/(m^2·K) to 50 W/(m^2·K), the decrease in hotspot temperature is nearly five times the result when h changes from 50 to 400 W/(m^2·K). This implies that once the convection coefficient reaches a certain level, further increases will only have a weak impact on the hotspot temperature. Besides, it is evident that the results obtained by FLUENT, the standard FVM, and the proposed method are well-aligned and the maximum absolute error between the proposed method and FLUENT is only 0.167 K. Therefore, we do not need to add more terms in the rational expression of the flexible TCM.

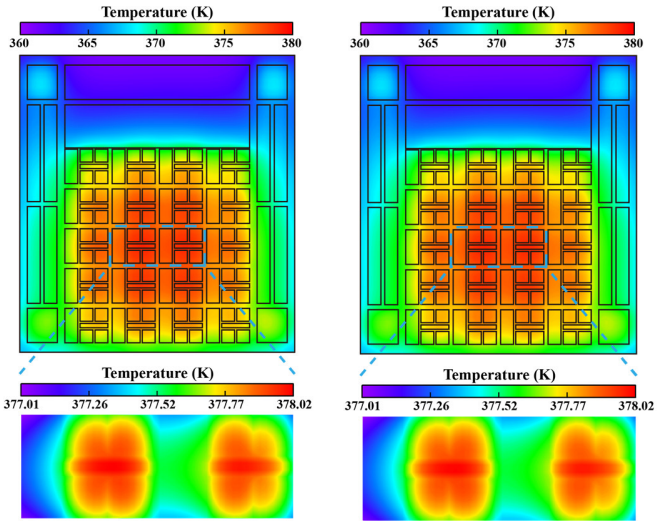

Fig. 8. Temperature distribution of the horizontal cross-section of the SoC die obtained by (a) FLUENT and (b) the proposed method.

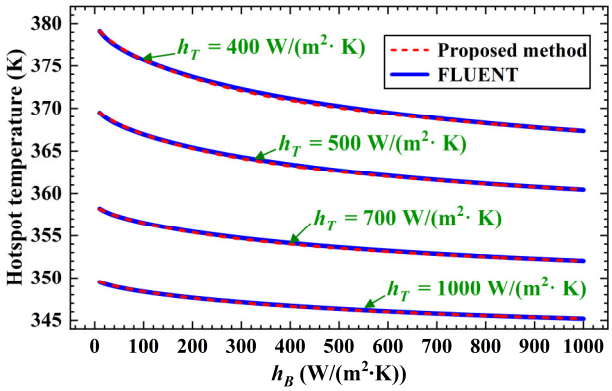

Fig. 9. Effect of convection coefficients h_T and h_B on the hotspot temperature.

In terms of efficiency, the CPU times for simulating all the 686 cases are compared in Table I. The establishment of the flexible TCM is regarded as a pre-simulation procedure and needs to be performed only once during the entire thermal design. The results show that the proposed method achieves a speedup of 138x compared to FLUENT and 100x faster than the standard FVM.

B. High-Performance Server SoC

In the second example, a more practical case of a high-performance server SoC is considered. The cross-section of the entire system is displayed in Fig. 6 and the geometric dimensions and material properties are referred to [11]. The floor-planning of the die is based on a commercial SoC, as outlined in [12]. The 3-D display of the SoC is shown in Fig. 7 and the power distribution originates from [13]. The top surface of the heat sink and the bottom surface of the PCB are set as convection boundaries with the coefficients of h_T and h_B, respectively and an ambient temperature of 300 K. All other surfaces are assumed to be adiabatic.

The objective of the thermal analysis in this example is to investigate the effect of h_T and h_B on the hotspot temperature.

TABLE II
EFFICIENCY PERFORMANCE UNDER THREE DIFFERENT MESHES

	DoFs			CPU Time			Speedup
	ROFs		ROI	Proposed method		FLUENT	
	Top	Bottom		Pre-simulation (Top ROF/Bottom ROF)	Simulation		
Mesh1	49,498	45,548	8,316	1 m 21 s / 1 m 6 s	28 m 8 s	2 h 55 m 1 s	6x
Mesh2	240,938	205,350	17,820	15 m 28 s / 10 m 28 s	29 m 24 s	16 h 35 m 33 s	18x
Mesh3	383,848	400,860	23,760	23 m 25 s / 28 m 1 s	34 m 42 s	30 h 8 m 20s	**21x**

Therefore, the whole system is divided into three parts: 1) ROI containing the TIM1, die, back-end-of-line (BEOL), and C4 micro-bump; 2) top ROF including the heat sink, pedestal, TIM2, and heat spreader; and 3) bottom ROF encompassing the substrate, solder balls with under filler, and PCB.

For accuracy verification, we simulate a typical case (h_T = 400 W/(m^2·K), h_B = 10 W/(m^2·K)) using FLUENT and the proposed method, respectively. The temperature profile of the horizontal cross-section in the SoC is depicted in Fig. 8. The results match remarkably well with each other. Fig. 9 demonstrates the effects of h_T and h_B on the hotspot temperature. When h_B = 400 W/(m^2·K), as h_T increases from 400 W/(m^2·K) to 1000 W/(m^2·K), the hotspot temperature decreases by nearly 24 K. However, when h_T = 400 W/(m^2·K), as h_B increases from 400 W/(m^2·K) to 1000 W/(m^2·K), the hotspot temperature only drops by less than 4 K. It indicates that the influence of h_T on the hotspot temperature is much more significant than that of h_B. Again, the results showcase good consistency and the maximum absolute error between the proposed method and FLUENT is only 0.22 K. Note that, similar to the first example, only one term is utilized in the rational expression of the flexible TCM.

As for efficiency, the CPU time comparison for the thermal simulations with three different meshes is presented in Table II. Since the top ROF and the bottom ROF are separated in space, the construction of their flexible TCMs can be implemented in parallel to further improve efficiency. In this example, 700 cases are simulated for thermal design. We obtain that with the increase in degrees of freedom (DoFs), the acceleration of the proposed method becomes more significant. Particularly, when the DoFs are 808,468 (383,848 + 400,860 + 23,760), the proposed method achieves a speedup of 21x compared to FLUENT. Note that the advantage of the flexible TCM-based approach will be more prominent with the increasing number of cases investigated in the thermal design.

IV. CONCLUSION

In this paper, the flexible TCM is proposed to perform efficient thermal simulation of 3-D ICs and packages. Following the principle of region decomposition, a novel technique based on the TCM has been developed. With the elegant rational expressions, the flexible TCM efficiently and accurately characterizes the properties of the ROF under varying convection boundary conditions. Due to the equivalent boundary conditions constructed by the flexible TCM, we focus the solution domain on the ROI, thereby accelerating the simulation and enabling fast thermal design. Compared to the commercial software FLUENT, the numerical results demonstrate a remarkable speedup of 138x achieved by the proposed method.

V. ACKNOWLEDGMENT

This work was supported by National Natural Science Foundation of China (62131014, 62188102) and Program of Shanghai Academic/Technology Research Leader (23XD1401800).

REFERENCES

[1] A. Rahman and R. Reif, "System-level performance evaluation of three-dimensional integrated circuits," *IEEE Trans. Very Large Scale Integr. (VLSI) Syst.*, vol. 8, no. 6, pp. 671–678, 2000.

[2] S. M. Alam *et al*., "Interstratum connection design considerations for cost-effective 3-D system integration," *IEEE Trans. Very Large Scale Integr. (VLSI) Syst.*, vol. 18, no. 3, pp. 450–460, 2010.

[3] A. Jain *et al*., "Analytical and numerical modeling of the thermal performance of three-dimensional integrated circuits," *IEEE Trans. Compon. Packag. Technol.*, vol. 33, no. 1, pp. 56–63, 2010.

[4] S. S. Salvi and A. Jain, "A review of recent research on heat transfer in three-dimensional integrated circuits (3-D ICs)," *IEEE Trans. Compon. Packag. Technol.*, vol. 11, no. 5, pp. 802–821, 2021.

[5] L. Codecasa *et al*., "A priori error bound for moment matching approximants of thermal models," *IEEE Trans. Compon. Packag. Technol.*, vol. 9, no. 12, pp. 2383–2392, 2019.

[6] L. Codecasa *et al*., "Fast novel thermal analysis simulation tool for integrated circuits (FANTASTIC)," in *20th International Workshop on Thermal Investigations of ICs and Systems*, Sep. 2014, pp. 1–6.

[7] L. Codecasa *et al*., "Galerkin's projection framework for BCI CTMs – Part I: extended FANTASTIC approach," *IEEE Trans. Compon. Packag. Technol.,* vol. 11, no. 11, pp. 1792-1803, 2021.

[8] S. Lan *et al*., "Thermal resistance network derivative (TREND) model for efficient thermal simulation and design of ICs and packages," in *61st ACM/IEEE Design Automation Conference (DAC)*, San Francisco, CA, USA, Jun. 2024.

[9] M. B. B. Hamida *et al*., "A three-dimensional thermal analysis and optimization of square light edding diode subcomponents," *Int. Commun. Heat Mass Transfer*, vol. 120, p. 105016, 2021.

[10] *ANSYS FLUENT Software* [Online]. Available: https://www.ansys.com/products/fluids/ansys-fluent.

[11] N. Kumar *et al.*, "Thermal analysis of high-performance server SoCs from FinFET to nanosheet technologies," in *2024 IEEE International Reliability Physics Symposium (IRPS)*, 2024, p. 8B.4-1-8B.4-8.

[12] *Ampere® Altra®* 64-Bit Multi-Core Processor [Online]. Available: https://d1o0i0v5q5lp8h.cloudfront.net/ampere/live/assets/documents/Altra_Rev_A1_PB_v1.35_20220728.pdf.

[13] R. Christy *et al.*, "8.3 A 3GHz ARM Neoverse N1 CPU in 7nm FinFET for infrastructure applications," in *2020 IEEE International Solid-State Circuits Conference (ISSCC)*, San Francisco, CA, USA, 2020, pp. 148–150.